Sustainable Energy & Fuels

Rapid Scalable Fabrication of Roll-to-Roll Slot-die Coated Flexible Perovskite Solar Cells Using Intense Pulse Light Annealing

Journal:	*Sustainable Energy & Fuels*
Manuscript ID	SE-ART-07-2022-000911.R1
Article Type:	Paper
Date Submitted by the Author:	18-Sep-2022
Complete List of Authors:	Chandrasekhar, Pakanati; University of Louisville, Conn Center for Renewable Energy Research Chapagain, Sashil; University of Louisville, Chemistry Martin, Blake; University of Louisville, Conn Center for Renewable Energy Research Armstrong, Peter; University of Louisville, Chemistry Grapperhaus, Craig; University of Louisville, Chemistry Druffel, Thad; University of Louisville, Conn Center for Renewable Energy Research

Rapid Scalable Fabrication of Roll-to-Roll Slot-die Coated Flexible Perovskite Solar Cells Using Intense Pulse Light Annealing

P. S. Chandrasekhar[1], Sashil Chapagain[2], Martin Blake[1], Peter Armstrong[2], Craig Grapperhaus[2]

and Thad L. Druffel[1]

[1]Conn Center for Renewable Energy Research, University of Louisville, Louisville, Kentucky, 40292, USA

[2]Department of Chemistry, University of Louisville, Louisville, Kentucky, 40292, USA

Email: pschandrasekhar9@gmail.com and thad.druffel@louisville.edu

Abstract

The perovskite solar cell has achieved high efficiencies at the lab scale using batch processes that often may not scale. Process that can be integrated in a continuous manufacturing platform, such as roll-to-roll, where several processes can be carried out sequentially are necessary to produce a new cost-competitive solar technology. In this work, IPL thermal post-processing is coupled with scalable slot-die coating and air knife evaporation in a high-speed roll-to-roll process of up to 2 m/min. Optimization of IPL energy parameters, web speeds, solution flow rates, and concentration of precursor inks yielded a champion power conversion efficiency of 11.24% for a 1 cm^2 roll-to-roll coated device. The overall processing time for a single layer in this process is reduced from minutes to seconds and the overall footprint of the manufacturing process is decreased. This demonstrates the promising capabilities for IPL to reduce manufacturing costs and paves a roadmap for scalable and efficient PSCs on a roll-to-roll platform.

Key words: Tin oxide, perovskite, roll-to-roll, slot-die coating, Intense Pulse Light, perovskite solar cells.

1. Introduction

Organic-inorganic hybrid perovskite solar cells (PSCs) have captured a tremendous interest in the photovoltaic community due to their excellent optoelectronic properties including tunable bad gap, high light absorption, long carrier diffusion lengths, high charge carrier mobility, and low nonradiative recombination losses. Moreover, these PSCs offer advantages of cost-effectiveness, ease of fabrication and remarkable power conversion efficiencies (PCEs) [1-6]. The fabrication of large area depositions has been demonstrated using several techniques such as inkjet printing[7, 8], gravure printing[9, 10], spray deposition[11, 12], doctor-blade coating[13, 14], slot-die coating[15, 16], and vapor deposition [17, 18] which have been adopted for roll-to-roll[19, 20] and sheet-to-sheet[21] platforms. Among these, slot-die coating is a suitable deposition technique for high volume production using high speed roll-to-roll industrial manufacturing on wide webs and has been demonstrated for perovskite films and charge transporting layers in a cost-effective mass production over rigid and flexible substrates at ambient conditions [22, 23]. The advantages of the slot die capabilities include very high-speed operation and uniform coating thickness across the web. Galagan *et al* demonstrated a slot die deposited SnO_2 electron transport layer (ETL) on a indium tin oxide coated polyethylene terephthalate substrate (PET/ITO) followed by a triple cation perovskite device with a PCE of 13.5% on an active area of 0.09 cm^2 using a fast-drying technique and optimized solvents [24].

The speed of roll-to-roll deposition of solution phase chemistries for the PSC relies on the evaporation of solvents and film transformations that are often carried out in ovens. Methods that can decrease the dwell times for these operations can further improve the economics of the PSC [25]. Radiative thermal processes, such as NIR-flash annealing, rapid thermal annealing, and intense

pulsed light (IPL), exhibit promising abilities to reduce dwell times [26-28]. In particular, IPL can reduce the dwell times from minutes to less than one second and can be implemented in-line with other roll-to-roll processes. IPL produces high intensity light pulses over a broad spectrum ranging from ultraviolet to near infrared from a Xenon lamp inducing high temperatures in large area films lasting just a fraction of a millisecond. Due to the rapidity of the process, IPL can be implemented on a roll-to-roll platform using a very small footprint for high speed operation. IPL has been used for sintering metallic (Copper and Silver) coatings on PET substrates and for thin-film enabled transistors and batteries [29-33]. More recently, IPL has been established for the processing of perovskite and other charge transport layers for the fabrication of efficient PSCs by eliminating conventional thermal processing. Lavery *et al*[34] annealed a two-step deposited perovskite film in 2 ms using the IPL technique, and A. H. Ghahremani *et al*[35] used an IPL gradient flash annealing obtaining superior morphology and high crystallinity of spin coated perovskite ($CH_3NH_3PbI_3$) films. S. Das *et al*[36] has used IPL technique for achieving high conductive TiO_2 layer over flexible PET substrates and R. T. Piper *et al*[37] used IPL for obtaining direct conversion of NiOx from sol-gel precursors for hole transport layer and to crystallize photoactive $MAPbI_3$ layers on flexible willow glass substrates.

In this work, IPL thermal post-processing is demonstrated in line with a slot-die coating and a rapid evaporation via an air knife process for a continuous high-speed roll-to-roll operation as shown in figure 1. A polymer web (PET/ITO) is continuously transported through each of the processes between the unwind and rewind stations at a constant speed. The web is a continuous flexible substrate that is conveyed between an unwind and rewind station at a constant speed where functional films are created in successive processes. The air knife is utilized to evaporate the solvents, and the IPL is used as a means to thermally process the layers. Two layers are

demonstrated in this continuous operation: SnO_2 as an electron transport layer (ETL) on PET/ITO followed by a perovskite ($MAPbI_3$) as an active absorbing layer. The optimization of the IPL process, solution flow rates, and concentration of precursor inks for web speeds up to 2 m/min were carried out to attain uniformity over a large area for high quality of SnO_2 and perovskite films. All the processing for this study were prepared in an ambient environment having humidity ≥ 40%. An inline corona discharge treater (CDT) is used to clean and increase the surface energy of the web. The thin films were analyzed using scanning electron microscopy (SEM), ultraviolet and visible spectroscopy (UV-Vis) and X-ray diffraction (XRD), where the latter two were also used to study the uniformity across and down the web. Devices measuring 1 cm^2 were built and characterized using I-V, resulting in champion device power conversion efficiency of 11.24%.

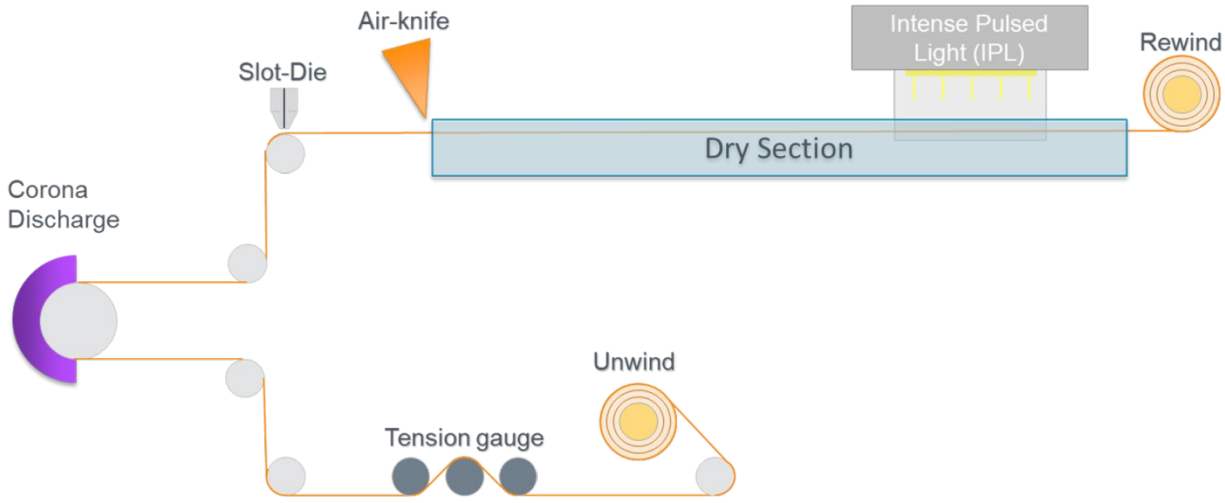

Figure 1. Schematic illustration of custom-built roll-to-roll machine setup showing the continuous processing between the unwind and rewind stations including CDT surface preparation, deposition by slot die, drying by an air knife and thermal processing using IPL.

2. Experimental section

Roll to Roll coating: Roll-to-roll depositions and IPL of electron transport and active perovskite layers were carried out using a custom designed roll-to-roll machine built and maintained by the Conn Center for Renewable Energy Research at the University of Louisville. The speed and tension of the web is maintained by two Mitsubishi motors controlled by a PLC. An ITO coated PET substrates (50 Ohm/sq) having 15 cm web width is used on the roll-to-roll coater which is equipped with CDT (EnerCon CoronaFlex) for surface treatment, slot-die (Premier Dies), air-knife pass drying unit (ExAir), and an Intense Pulse Light (IPL) (Xenon Corp. S2210) as shown in Figure 1. All of the processes are done at a constant web speed.

2.1 Processing of SnO_2 as an electron transport layer:

The SnO_2 films were deposited over CDT ITO coated PET substrates under ambient conditions using. A CDT is often used with roll-to-roll depositions to increase the surface energy of a web surface such that it exceeds the surface tension of the chemistry which improves wetting. The SnO_2 precursor ink was prepared by diluting the SnO_2 colloidal dispersion (Alfa Aesar, 15 wt.%) with DI water and anhydrous ethanol in a vol. ratio of 2:1 containing 12 µl of Triton-X 100 surfactant. Prior to the deposition, the solution was stirred for 2 h, sonicated for 20 min, and filtered through a 20 µm cellulose syringe filter. As obtained SnO_2 solution was deposited by slot-die coating with at 25 micron thick shim at a web speed of 2 m/min, meniscus gap of 50 µm, flow rate of 1.8 ml/min, followed by an air-knife drying (~30 psi) and IPL process having energy density of 1.22 J/cm^2 (1940 V), duration of 1000- µsec and delay time of 200 msec.

2.2 Processing of perovskite layer:

The perovskite precursor solution consists of an equimolar ratio (0.6 M) of methyl ammonium iodide (MAI) and lead iodide (PbI_2) were dissolved in a mixed solvent of 3:2 vol. ratio of acetonitrile (ACN) and 2-Methoxy ethanol (2-ME), subjected to stirring for 2 h in a glove box. 20 mol% of L-α-phosphatidylcholine (LP) surfactant and DMSO were added to the solution prior to deposition. The deposition was carried out using a slot-die coater having a 25 micron thick shim at a web speed of 1.8 m/min meniscus gap of 50 mm, flow rate of 1.6 ml/min followed by a an air-knife drying (~20 psi) and IPL process at 1500 V, duration of 600 µsec and delay time of 1000 msec. The temperature and relative humidity are in the average range of 25 to 30 °C, and ≥40 %, respectively.

2.3 Device fabrication:

As roll-to-roll coated SnO_2 and perovskite films were taken off the web and sliced into suitable small pieces for the device fabrication containing an active area of 1 cm^2. The device fabrication is completed after spinning the Spiro-OMeTAD solution as a hole transporting layer (HTL) and thermal evaporation of Molybdenum oxide (MoO_X) as a buffer layer and final top Ag contacts. The HTL was deposited by spinning Spiro-OMeTAD solution over roll-to-roll deposited perovskite films at a speed of 2000 rpm for 40 s. The Spiro-OMeTAD solution was prepared by dissolving 144 mg of p,o-spiro-OMeTAD (Lumtec) in 2ml of Chlorobenzene, 58 µl of 4-tert-butylpyridine, 35 µl of a 520 mg ml^{-1} Li-TFSI solution in acetonitrile and 58 µl of a 500 mg ml-1 FK209 cobalt salt in acetonitrile were also added. Subsequently, the substrates were transferred to the thermal evaporator under the pressure of 2.0×10^{-6} mbar, where 8 nm of MoOx as a buffer

layer and 80 nm of Ag back electrode were deposited on top of the Spiro-OMeTAD film. The Ag electrodes were evaporated with shadow custom designed masks for determining the active area of the device, which is 1cm^2.

2.4 Characterization:

The roll-to-roll coated SnO_2, and perovskite film thicknesses were measured using a Veeco Dektak 3M stylus surface profilometer. UV–visible absorption was carried out using an Agilent Carry UV- spectrometer. XRD measurements were carried out using a D8 Rigaku instrument equipped with Cu Kα radiation of 1.54 Å. Scanning Electron Microscopy (SEM) images were captured using a Thermo Scientific. The J-V curves of PSCs were measured using a Keithley 2400 source meter at room temperature. The light source was a solar simulator (Oriel class AAB) was equipped with a 1000 W tungsten lamp to match AM 1.5 G. The intensity of the light (100mW/cm^2) was calibrated by a standard silicon reference solar cell (SolarMade standards, NREL certified). The devices are having an active area of 1 cm^2 and scanned in both light and dark conditions in the range of 0 to 1.2 V at a scan speed of 100 mV/s.

3. Results and Discussion

In roll-to-roll scalable production, a key factor for achieving highly efficient PSCs is creating uniform, large area charge transport layers and the photoactive perovskite layer on a continuously moving high speed web. The roll-to-roll processing of the films in this work consist of three steps: (a) slot-die coating of precursor solution, (b) solvent evaporation from the wet film using an air-knife, and (c) thermal processing using IPL. Each step is time-sensitive and must be optimized to the continuous web, where the slowest process defines the overall web speed. The optimization of the inks, deposition and drying are summarized here, with most of the details left to the supporting

information (SI), since the focus of the work is integrating the IPL into a continuous roll-to-roll production. Control of the evaporation includes changes to the solvent systems (higher vapor pressure solvents) and the use of forced convection (air knives). Faster evaporating solvents will allow for a faster web speed. Solvents such as water and dimethylformamide (DMF) have low vapor pressures and can thus prolong the evaporation process, which can slow web speeds or increase the overall footprint of the process. The SnO_2 inks employed alcohols and the perovskite inks adopted a co-solvent system of 3:2 vol. ratio of ACN:2-MeOH for achieving both fast drying and large perovskite crystal grains at room temperature [16, 38-40]. Both inks also utilized surfactants to improve the wetting during deposition. The slot die deposition requires that the flow rate of the inks, web speed and gap between the tool and the web are balanced in order to maintain a consistent meniscus to achieve a uniform coating. These refinements ensure that a uniform dry film is translated into the IPL for thermal processing. In this study, all the films and corresponding devices are fabricated in a continuous process by using solution processing of slot-die coating deposition over 15 cm ITO coated PET films at ambient conditions, with evaporation occurring using a 15 cm wide air knife, and thermally processed using an IPL unit with a 15 cm x 15 cm processing area.

3.1. Optimizing different IPL conditions:

The spectrum of the Xenon lamp is from 300 to 1100 nm and the intensity of the energy is manipulated by the voltage applied across the lamp and the length of the pulse [41]. The optimization of the IPL parameters includes the energy density (J/cm^2), pulse width (μs) and pulse delay (ms). The energy density and the pulse width are tuned to deliver sufficient energy without damaging the films or the underlying substrate. The control of the pulse delay is to time the pulses such that the thin films will be exposed to multiple pulses as the web passes through the IPL unit where the

frequency of the flashes is the inverse of the delay time. The IPL unit has an optical window of 15 cm by 15 cm, and it is advantageous to flash the lamps such that each section of the moving web is exposed to multiple flashes to ensure a uniform heating. Thus, the number of flashes the films are exposed to is equal to the length of the window (15 cm) divided by the web speed multiplied by the frequency of the lamp. The spectrum of the lamp output and the description of the pulse train is shown in Figure S10.

The deposition and thermal processing of SnO_2 in roll-to-roll manufacturing has been caried out where the thermal processing is accomplished in an oven and improves the performance of the devices [42, 43]. The IPL can be used to replace the oven, where the optimization of the IPL process involves multiple pulses as the web translates under the light source. The use of IPL with a SnO_2 thin film for perovskites has previously been shown to maximize the binding energy of the Sn $3d_{5/2}$ which leads to an improved charge transfer [44]. That work utilized glass as the substrate, which has a higher thermal mass which will require higher energy densities. In this work, the IPL processing of the SnO_2 layer was optimized considering energy densities of 0.85, 1.22 and 2.13 J/cm^2. The delay time of 200 msec was chosen such that at 2 m/min the film would be exposed to as many pulses as possible (>20) to ensure that the films are completely processed. SEM images of the surface of the SnO_2 films after the IPL processing are shown in figure 2. It is clear from these images that at the energy density of 2.1 J/cm^2, the films have cracked indicating that the energy was too high. It was also observed that the films at 0.85 J/cm^2 exhibited scratches from the rewind process indicating that the energy was too low. Thus, the optimal response was determined to be 1.22 J/cm^2 as this condition bridged the processing window.

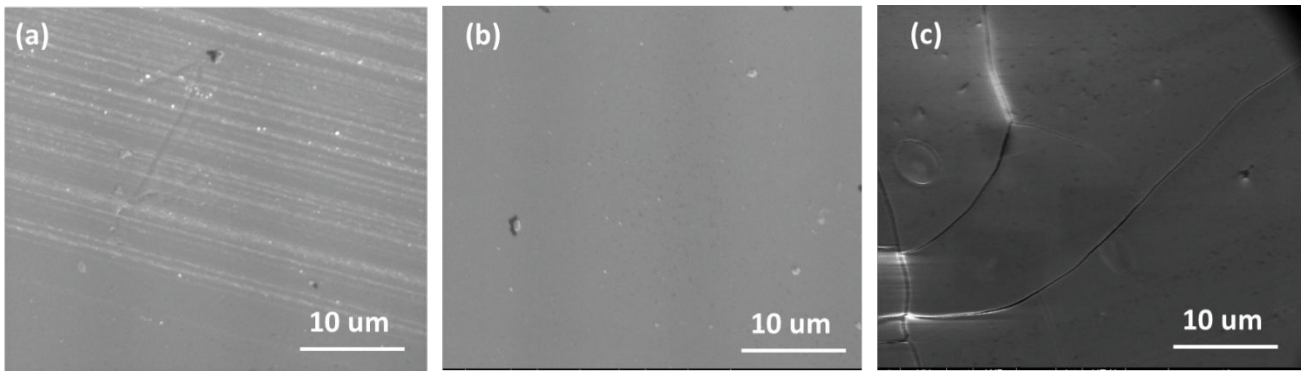

Figure 2: SEM images of roll-to-roll slot-die coated SnO_2 films processed at three different IPL energy densities (a) 0.85, (b) 1.22, and (c) 2.13 J/cm^{2,} respectively.

Similarly, the deposition and thermal processing of a perovskite thin film has been carried out where using an oven to accomplish the thermal annealing [22, 24, 45]. The IPL process can replace the oven and since the perovskite film absorbs light energy very well it requires an overall lower energy than SnO_2. Thus, the number of pulses and energy density of each pulse can be reduced. During optimization, different IPL annealing conditions were carried out as listed out in Table 1 by varying different energies and duration of pulses to achieve quality perovskite films. For each set of conditions, corresponding labeling is given as IPL# A, B, C, D, E, and F respectively. The pulse delay time of 1,000 msec was kept constant and chosen such that the perovskite film was exposed to 5 pulses of energy to ensure an even annealing over the moving web.

Table 1. Different IPL conditions processed for roll-to-roll slot-die coating of perovskite film

Optimization of IPL	Potential (V)	Energy density (J/cm^2)	Duration (µsec)	Delay (msec)
IPL# A	2000	1.57	500	1000
IPL# B	1850	1.52	600	1000
IPL# C	1750	0.86	500	1000
IPL# D	1600	0.78	500	1000
IPL# E	1500	0.74	600	1000
IPL# F	1350	0.65	500	1000

From the figure 3 it is seen that there is complete degradation of perovskite film for the condition of IPL# A. It is attributed to the generation of high heat flux at stronger pulses with high energy value of 1.57 J/cm^2 and the corresponding morphology is shown as needle like structure of dissociated perovskite precursor composition. As the energy values are decreased further from IPL# B to IPL# F, it was found a gradual transition from cracked, pale, yellow-colored films to a uniform dark film with a formation of crystalline perovskite films having minimal pinholes. Thus, the case of IPL# E condition remains as the optimal annealing condition for obtaining quality perovskite films with an improved crystallinity and high surface coverage. At the lower energy density value of IPL# F resulted in a film quality that was poor exhibiting agglomeration of small crystals along with large voids.

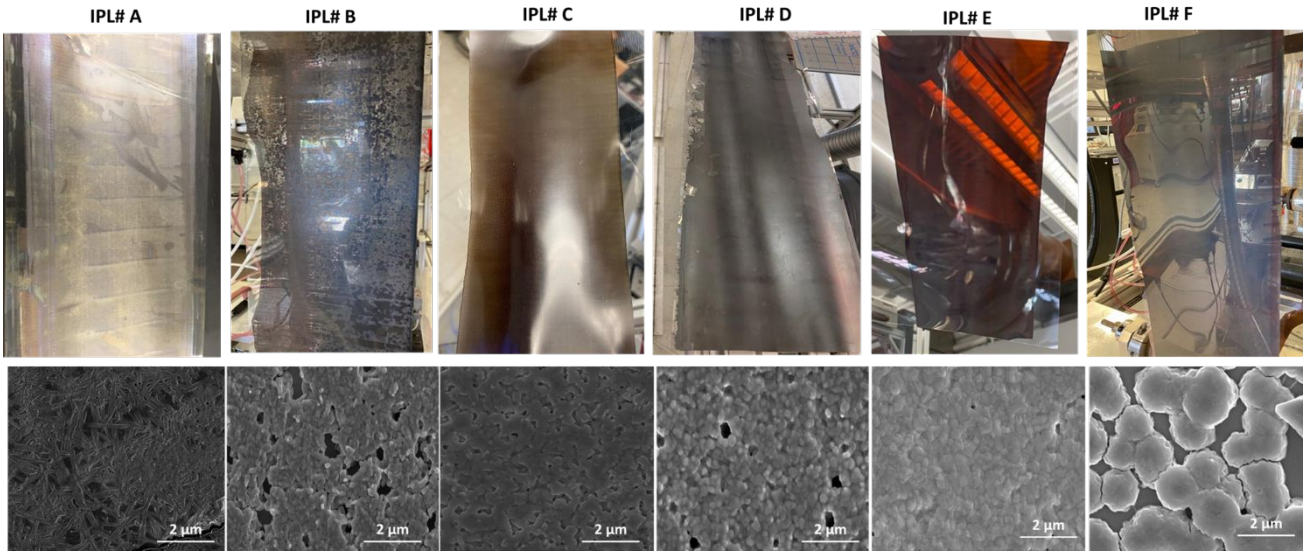

Figure 3: Optical and SEM images of roll-to-roll deposited perovskite films processed at different IPL conditions.

Thus, at the optimized conditions of IPL, and web speed, a suitable slot-die coating of uniform perovskite and SnO_2 films are achieved with an average thickness of 940 nm, and 72 nm, and their surface roughness are found to be 25 nm and 8 nm, respectively. The perovskite coating thickness is more than the optimal 500 nm which is due primarily to high level coating non-uniformities as the layer was reduced due to the roughness of the ITO. More work is required to reduce this layer thickness, primarily towards smoothing the interface between the ITO and perovskite. Optical images of as deposited perovskite films are shown in Figure 4a and 4b and SEM images are shown in Figure 4c and 4d. The slot-die coated perovskite films exhibit a compact and uniform layer with an average crystal size of ~450 nm (A video demonstrating the roll-to-roll deposition of perovskite film is presented in electronic supplementary information). The process parameters for both the SnO_2 and perovskite films are shown in table 2. The IPL accomplishes the thermal processing of SnO_2 and perovskite films in fraction of seconds in line on a continuous high web speed and has a very small footprint.

Table 2. Deposition parameters of SnO_2 and $MAPbI_3$ films by roll-to-roll slot-die coating and the corresponding post-treatment of IPL energy values.

Thin film (material)	Speed (M/min)	Flow rate (ml/min)	Gap (um)	CDT (kW)	Energy (J/cm2)	Voltage (V)	Duration (μsec)	Delay (msec)
SnO_2	2.0	1.8	50	0.35	1.22	1940	1000	200
$MAPbI_3$	1.8	1.6	40	0.20	0.74	1500	600	1000

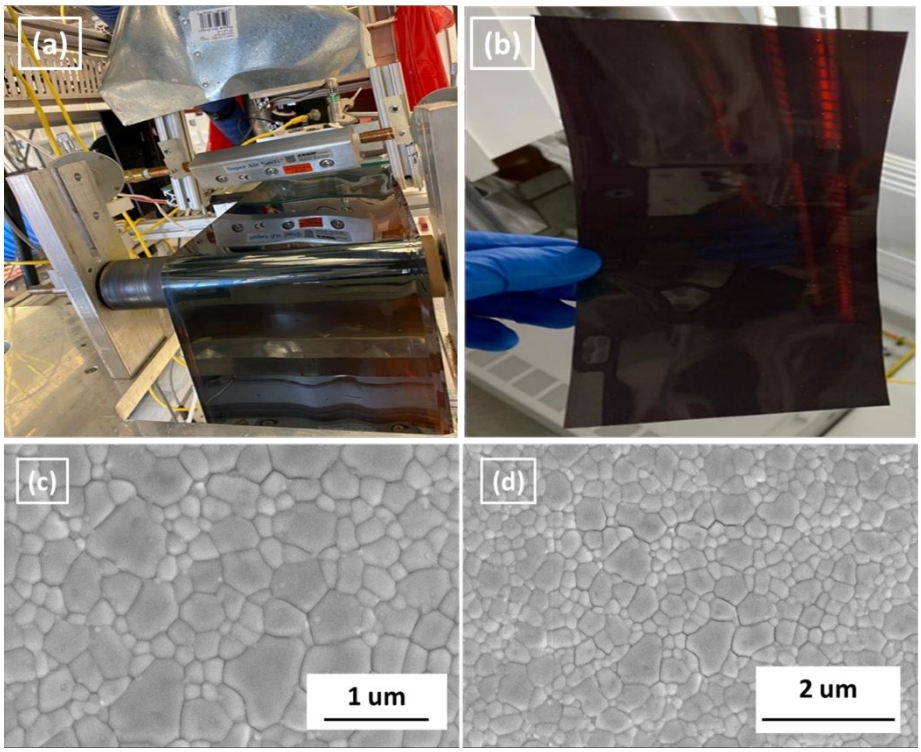

Figure 4. Optical (a and b) and SEM (c and d) images of roll-to-roll slot-die coated perovskite films by IPL thermal post processing.

3.2 Uniformity

Samples were collected at locations across the web (orthogonal to web movement spanning 15 cm width) and down the web (parallel to web movement over a 2m length) of IPL processed perovskite

films as shown in figure 5a. Thickness measurements of the perovskite film yielded an average 940 ± 21 nm. UV-Visible absorption, and X-ray diffraction (XRD) analysis were also done on these samples and their corresponding spectra are shown in Figure 5b and 5c. The absorption profiles in figure 5b show a very similar distributions further verifying the uniform thickness as well as demonstrating a uniform annealing. The XRD spectra exhibited the same peak at 14.2^0 corresponding to (110) crystal plane of the tetragonal phase of perovskite structure from all the samples, and no other additional peaks were detected. These data demonstrate that the thickness of the perovskite and crystalline structure of the slot die, IPL process films from the continuous web were uniform.

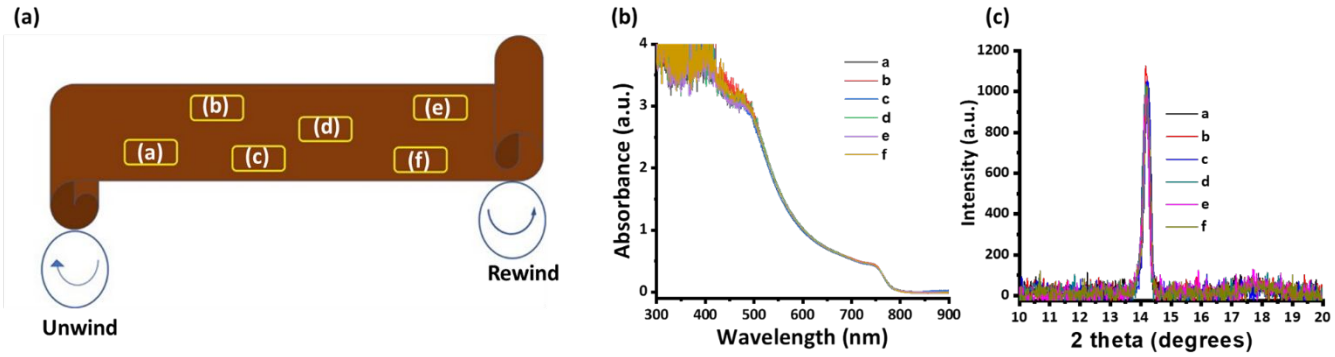

Figure 5. Roll-to-roll slot-die coated perovskite film, a) optical image of specifying different random locations of the web, b) and c) corresponding Uv-Visible absorption and XRD spectra.

3.3 Photovoltaic performance

Solar cell devices were assembled from the optimized roll-to-roll slot die coated and IPL processed SnO_2, and perovskite films chosen from the five locations across and down the web as shown in figure 5a. The champion device exhibited a PCE of 11.24% with a V_{oc} of 0.91 V, Jsc of 23.7 mA/cm^2, and FF of 52 % over an active area of 1 cm^2 as shown in figure 6a. A statistical

distribution of the performance from the ten 1 cm^2 devices (active area 1 cm^2) collected from each of the five locations is shown in figure 6b. An average stabilized PCE of 10.6% was obtained with an average open circuit voltage (V_{oc}) of 0.97 V, current density (J_{sc}) of 22.9 mA/cm^2, fill factor (FF) of 47%. The corresponding photovoltaic parameters are summarized in Table 3. The FF and the Voc are lower than expected and can be attributed to the thickness of the perovskite and ITO layers. A thicker perovskite layer will reduce the FF and Voc due to a higher charge recombination. The thickness of the ITO layer on the PET yields a resistance of 50 Ω/sq and hence will decrease the FF as is evident from the slope of the J-V curve showing high series resistance.

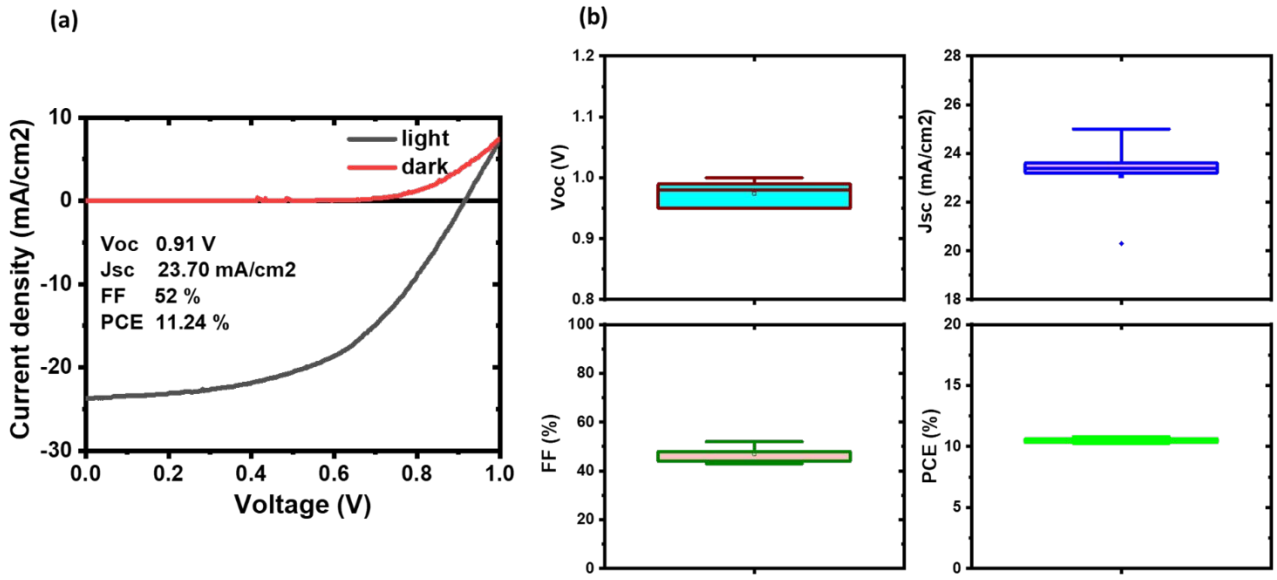

Figure 6. a) J-V curves of the champion devices measured under light and dark conditions for roll-to-roll SnO_2, and MAPI, and b) box plots of Voc, Jsc, FF an PCE for PSCs collected at different locations across the web.

Table 3. Statistical analysis of ten devices made at five locations across and down the web.

Location	Voc (V)	Jsc (mA/cm2)	FF (%)	PCE (%)
1	0.95 ± 0.02	23.40 ± 0.16	48 ± 1.87	10.64 ± 0.38
2	0.98 ± 0.01	23.20 ± 0.21	48 ± 1.91	10.82 ± 0.21
3	0.95 ± 0.03	24.10 ± 0.11	46 ± 2.12	10.56 ± 0.26
4	1.00 ± 0.01	20.30 ± 0.29	52 ± 1.21	10.51 ± 0.29
5	0.99 ± 0.02	23.60 ± 0.14	44 ± 2.32	10.33 ± 0.31

4. Conclusion

The large area depositions of SnO_2 and perovskite films using a slot die coating and IPL process inline on a continuously moving web was demonstrated. The optimization of the processing included varying web speeds, different solvent systems for perovskite inks and different IPL conditions and each of these play a significant role in attaining high quality films over large areas at high web speeds. The films were optimized for uniform thickness and crystallinity across a 15 cm wide web and down a 2 m section of web as demonstrated by thickness measurements, UV-vis spectroscopy and XRD. As resulting PSCs exhibited a champion PCE of 11.24 % with the average stabilized PCE of 10.57% for an active area of 1 cm^2 was obtained from random locations across the 15 cm web and 2 m length roll. This work paves a scalable method for a low-cost and efficient PSCs by employing IPL over roll-to-roll platform.

Acknowledgements

The authors would like to thank the Conn Center for Renewable Energy Research and Micro/Nano Technology Center at the University of Louisville for assisting in characterization of the samples. This work is funded in part or whole by the U.S. Department of Energy Solar Energy Technologies Office Award Number(s) DE-EE0008752.

References

1. H.-S. Kim, C.-R. Lee, J.-H. Im, K.-B. Lee, T. Moehl, A. Marchioro, S.-J. Moon, R. Humphry-Baker, J.-H. Yum, J. E. Moser, M. Grätzel and N.-G. Park, *Scientific Reports*, 2012, **2**, 591.
2. M. A. Green, A. Ho-Baillie and H. J. Snaith, *Nature Photonics*, 2014, **8**, 506-514.
3. J.-P. Correa-Baena, A. Abate, M. Saliba, W. Tress, T. Jesper Jacobsson, M. Grätzel and A. Hagfeldt, *Energy & Environmental Science*, 2017, **10**, 710-727.
4. E. M. Hutter, G. E. Eperon, S. D. Stranks and T. J. Savenije, *The Journal of Physical Chemistry Letters*, 2015, **6**, 3082-3090.
5. J.-P. Correa-Baena, M. Saliba, T. Buonassisi, M. Grätzel, A. Abate, W. Tress and A. Hagfeldt, *Science*, 2017, **358**, 739-744.
6. D. Stranks Samuel, E. Eperon Giles, G. Grancini, C. Menelaou, J. P. Alcocer Marcelo, T. Leijtens, M. Herz Laura, A. Petrozza and J. Snaith Henry, *Science*, 2013, **342**, 341-344.
7. F. Mathies, T. Abzieher, A. Hochstuhl, K. Glaser, A. Colsmann, U. W. Paetzold, G. Hernandez-Sosa, U. Lemmer and A. Quintilla, *Journal of Materials Chemistry A*, 2016, **4**, 19207-19213.
8. F. Mathies, E. J. W. List-Kratochvil and E. L. Unger, *Energy Technology*, 2020, **8**, 1900991.
9. Y. Y. Kim, T.-Y. Yang, R. Suhonen, M. Välimäki, T. Maaninen, A. Kemppainen, N. J. Jeon and J. Seo, *Advanced Science*, 2019, **6**, 1802094.
10. F. Bisconti, A. Giuri, R. Suhonen, T. M. Kraft, M. Ylikunnari, V. Holappa, R. Po', P. Biagini, A. Savoini, G. Marra, S. Colella and A. Rizzo, *Cell Reports Physical Science*, 2021, **2**, 100639.
11. M. Park, W. Cho, G. Lee, S. C. Hong, M.-c. Kim, J. Yoon, N. Ahn and M. Choi, *Small*, 2019, **15**, 1804005.
12. J. E. Bishop, J. A. Smith and D. G. Lidzey, *ACS Applied Materials & Interfaces*, 2020, **12**, 48237-48245.
13. A. S. Marques, R. M. Faria, J. N. Freitas and A. F. Nogueira, *Industrial & Engineering Chemistry Research*, 2021, **60**, 7145-7154.
14. Y. Xiao, C. Zuo, J.-X. Zhong, W.-Q. Wu, L. Shen and L. Ding, *Advanced Energy Materials*, 2021, **11**, 2100378.
15. R. Patidar, D. Burkitt, K. Hooper, D. Richards and T. Watson, *Materials Today Communications*, 2020, **22**, 100808.
16. J. Li, J. Dagar, O. Shargaieva, M. A. Flatken, H. Köbler, M. Fenske, C. Schultz, B. Stegemann, J. Just, D. M. Többens, A. Abate, R. Munir and E. Unger, *Advanced Energy Materials*, 2021, **11**, 2003460.
17. J. Feng, Y. Jiao, H. Wang, X. Zhu, Y. Sun, M. Du, Y. Cao, D. Yang and S. Liu, *Energy & Environmental Science*, 2021, **14**, 3035-3043.
18. R. Swartwout, M. T. Hoerantner and V. Bulović, *ENERGY & ENVIRONMENTAL MATERIALS*, 2019, **2**, 119-145.

19. J. F. Benitez-Rodriguez, D. Chen, M. Gao and R. A. Caruso, *Solar RRL*, 2021, **5**, 2100341.
20. H. Li, C. Zuo, A. D. Scully, D. Angmo, J. Yang and M. Gao, *Flexible and Printed Electronics*, 2020, **5**, 014006.
21. Y.-C. Huang, C.-F. Li, Z.-H. Huang, P.-H. Liu and C.-S. Tsao, *Solar Energy*, 2019, **177**, 255-261.
22. D. Burkitt, R. Patidar, P. Greenwood, K. Hooper, J. McGettrick, S. Dimitrov, M. Colombo, V. Stoichkov, D. Richards, D. Beynon, M. Davies and T. Watson, *Sustainable Energy & Fuels*, 2020, **4**, 3340-3351.
23. T.-Y. Yang, Y. Y. Kim and J. Seo, *APL Materials*, 2021, **9**, 110901.
24. Y. Galagan, F. Di Giacomo, H. Gorter, G. Kirchner, I. de Vries, R. Andriessen and P. Groen, *Advanced Energy Materials*, 2018, **8**, 1801935.
25. B. Martin, D. Amos, E. Brehob, M. F. A. M. van Hest and T. Druffel, *Applied Energy*, 2022, **307**, 118200.
26. S. Sánchez, M. Vallés-Pelarda, J.-A. Alberola-Borràs, R. Vidal, J. J. Jerónimo-Rendón, M. Saliba, P. P. Boix and I. Mora-Seró, *Materials Today*, 2019, **31**, 39-46.
27. S. Sánchez, J. Jerónimo-Rendon, M. Saliba and A. Hagfeldt, *Materials Today*, 2020, **35**, 9-15.
28. B. Martin, M. Yang, R. C. Bramante, E. Amerling, G. Gupta, M. F. A. M. van Hest and T. Druffel, *Materials Letters*, 2020, **276**, 128215.
29. R. Dharmadasa, M. Jha, D. A. Amos and T. Druffel, *ACS Applied Materials & Interfaces*, 2013, **5**, 13227-13234.
30. K. Ankireddy, T. Druffel, S. Vunnam, G. Filipič, R. Dharmadasa and D. A. Amos, *Journal of Materials Chemistry C*, 2017, **5**, 11128-11137.
31. M. Kim, H. Jee and J. Lee, *Nanomaterials*, 2021, **11**.
32. H. J. Kim, C. J. Han, B. Yoo, J. Lee, K. Lee, K. H. Lee and M. S. Oh, *Micromachines*, 2020, **11**.
33. X. Chen, J. Sastre, A. Aribia, E. Gilshtein and Y. E. Romanyuk, *ACS Applied Energy Materials*, 2021, **4**, 5408-5414.
34. B. W. Lavery, S. Kumari, H. Konermann, G. L. Draper, J. Spurgeon and T. Druffel, *ACS Applied Materials & Interfaces*, 2016, **8**, 8419-8426.
35. A. H. Ghahremani, S. Pishgar, J. Bahadur and T. Druffel, *ACS Applied Energy Materials*, 2020, **3**, 11641-11654.
36. S. Das, B. Yang, G. Gu, P. C. Joshi, I. N. Ivanov, C. M. Rouleau, T. Aytug, D. B. Geohegan and K. Xiao, *ACS Photonics*, 2015, **2**, 680-686.
37. R. T. Piper, T. B. Daunis, W. Xu, K. A. Schroder and J. W. P. Hsu, *Frontiers in Energy Research*, 2021, **9**.
38. Y. Deng, H. Van Brackle Charles, X. Dai, J. Zhao, B. Chen and J. Huang, *Science Advances*, **5**, eaax7537.
39. K. H. Hendriks, J. J. van Franeker, B. J. Bruijnaers, J. A. Anta, M. M. Wienk and R. A. J. Janssen, *Journal of Materials Chemistry A*, 2017, **5**, 2346-2354.
40. Y. Deng, C. H. Van Brackle, X. Dai, J. Zhao, B. Chen and J. Huang, *Science Advances*, **5**, eaax7537.
41. T. Druffel, R. Dharmadasa, B. W. Lavery and K. Ankireddy, *Solar Energy Materials and Solar Cells*, 2018, **174**, 359-369.
42. T. Bu, J. Li, F. Zheng, W. Chen, X. Wen, Z. Ku, Y. Peng, J. Zhong, Y.-B. Cheng and F. Huang, *Journal*, 2018, **9**, 4609.
43. M. S. Kiani, Z. T. Sadirkhanov, A. G. Kakimov, H. P. Parkhomenko, A. Ng and A. N. Jumabekov, *Nanomaterials (Basel, Switzerland)*, 2022, **12**.
44. A. H. Ghahremani, B. Martin, A. Gupta, J. Bahadur, K. Ankireddy and T. Druffel, *Materials & Design*, 2020, **185**, 108237.
45. J.-E. Kim, Y.-S. Jung, Y.-J. Heo, K. Hwang, T. Qin, D.-Y. Kim and D. Vak, *Solar Energy Materials and Solar Cells*, 2018, **179**, 80-86.